MIT Bates Linear Accelerator Center Wind Energy Resource Assessment Project - Preliminary Analysis Report

Wind Energy Projects in Action (WEPA) team

Massachusetts Institute of Technology

Alex Kalmikov
Wind Data Analysis, Resource Assessment, Turbine Power Estimates

Yuewei Ji
Shadow Flicker and Community Impact Analysis

Maria Cassidy
GIS and Visualization

December 8, 2011

Acknowlegments

We would like to thank everyone who helped us with this report. Special thanks to:

Katherine Dykes for her leadership and guidance;

Cy Chan and Sungho Lee for technical advice and sharing data and codes;

Joanne McCarthy and staff of MIT Bates Linear Accelerator Center for weekly collection of wind data;

Steven Lanou of MIT Environmental Programs Office and Amanda Graham, Jennifer DiMase and Christie Ko of MIT Energy Initiative Education Office for support of WEPA activities;

NRG Systems for donation and installation of meteorological equipment.

1 Introduction

MIT Bates Linear Accelerator Center Wind Energy Resource Assessment project goals are to provide a quantitative assessment of the available wind energy resource at the Bates facility site and estimate its power generation potential as well as economic and environmental feasibility of possible projects. The site is located in Middleton, MA on top of a hill at 64±1m above mean sea level, coordinates +42° 35' 47.90", -70° 58' 42.66" (Latitude 42.596638, Longitude -70.978518). The topography of the site is complex. The hill is a dominant local topographic feature, elevated above the surrounding valleys more than 30 meters. The slopes of the hill are considerably steep with gradients order of 10%. Nonetheless, the hill is not isolated and is dominated by slightly higher (66m) and wide hill 2000 feet to the west. The land cover at the site is grass, surrounded by forest trees 200-300 feet from the meteorological tower location. Tall water tower is located 150 feet to north-west of the meteorological tower, which is the upwind direction of the wintertime dominant north-westerlies expected in the region[1].

Figure 1. Aerial photograph of the site, marked by blue arrow.

[1] Kalmikov A. et al., 2010, *Wind Power Resource Assessment in Complex Urban Environments: MIT Campus Case-Study Using CFD Analysis*, American Wind Energy Association WINDPOWER 2010 Conference, WEPA, MIT.

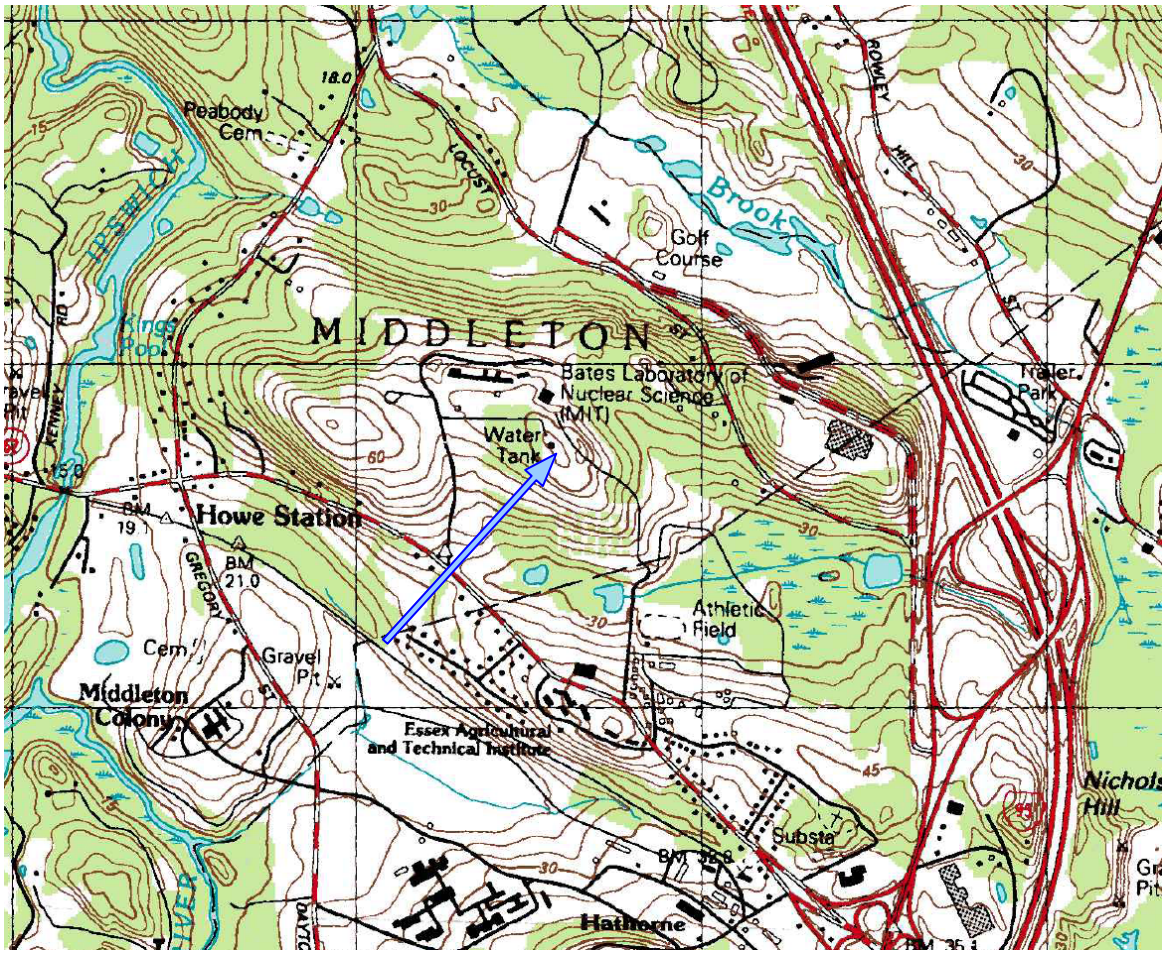

Figure 2. Topographic map of the site, elevation contours every 3m. The site is marked by blue arrow.

The preliminary analysis presented below addresses the climatology of winds measured at the site over one year period, the statistics of wind power potential, specific power production estimates for selected small to medium size turbines, and shadow flicker environmental impacts. Long term wind climatology, other environmental impacts, and the economic feasibility of turbine installation will be addressed in follow up reports.

2 Wind Resource Assessment

2.1 Data collection

Wind data was measured at the site with NRG 34m meteorological tower and recorded with NRG Symphonie Logger (see Appendix 1 for sensors specifications and calibration tables). Data from two sets of two anemometers and one wind vane were collected at two heights: 20 and 34 meters above the ground. Temperature sensor mounted 2.5m above the ground provided data used for air density calculations.

This report analyses the data collected during 1 year from November 3 2010 to November 7 2011. The collected data was inspected and filtered to remove anomalies, such as freezing of vanes and anemometers, with data recovery rate 98.9%. Tower shadow effect on anemometers was detected and filtered out (see Appendix 2). Overall, the sensors appear to have functioned as expected and no major faults detected.

2.2 Wind Power Density

Wind Power Density (WPD) is a standard quantitative measure of available wind energy, defined as the flow rate of kinetic energy of air through unit area cross section, i.e. the kinetic energy flux or kinetic power per unit area. WPD is measured in W/m^2 and is given by the formula

$$WPD = \tfrac{1}{2}\rho U^3 \tag{2.1}$$

Mean WPD is the instantaneous WPD averaged over a given period of time and represents the total wind energy available for harvesting[1]. Mean WPD is the quantitative basis for NREL wind power classification (see Appendix 3).

[1] Note, that it is impossible to harvest all this available energy because no existing turbine design can operate with 100% power efficiency. The fundamental limit to aerodynamic efficiency of wind turbines, as predicted by Betz theory, is 59%.

2.3 Wind Resource Analysis

Sample of raw unfiltered collected wind speed data, 10 minute averages at 34m height, is shown in Figure 3. Monthly averages of the processed wind speed data are shown for both measurement heights. These monthly averages are listed in Table 1, together with the best fit Weibull distribution parameters and monthly mean WPD. As expected wintertime winds are stronger, with WPD at 34m higher than 100 W/m^2. In summer months WPD at 34m is 50 W/m^2 and below, but note the anomalously high WPD during August 2011, clearly result of hurricane Irene (another indicator of this anomaly is the Weibull Shape parameter which is lower than during other summer months, while the mean wind speed is not much different - meaning that the distribution is skewed due to the strong hurricane winds).

Annual mean WPD is 92 W/m^2 at 34m and 52 W/m^2 at 20m above ground. Comparing to the standard NREL classification (Appendix 3) - the site has Wind Power Class 1, meaning "poor" resource potential. This is consistent with NREL regional map, which predicts only limited pockets of Wind Power Class 2 or "marginal" wind resource over this geographical area. Note, however, that the classification is based on WPD at the standard heights of 10 and 50 meters, and while our site is certainly class 1 based on winds expected at 10m, the winds at higher elevations may be stronger due to the speedup effects of the complex topography at the site (see the vertical extrapolation discussion below).

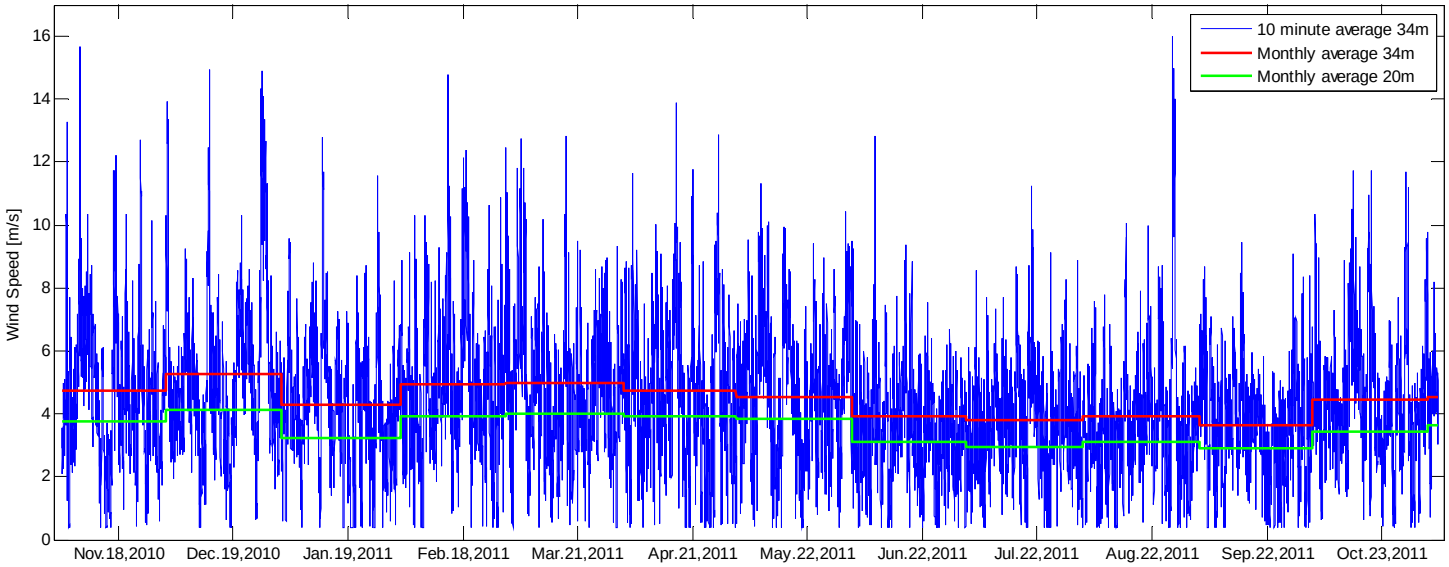

Figure 3: 1 year wind speed data (raw unfiltered 10 minute averages from channel 1) and filtered monthly averages at both measurement heights.

	Mean Wind 34m	Weibull Scale 34m	Weibull Shape 34m	Mean WPD 34m	Mean Wind 20m	Weibull Scale 20m	Weibull Shape 20m	Mean WPD 20m
Nov 2010	4.72	5.32	2.40	107	3.75	4.24	2.20	59
Dec 2010	5.28	5.97	2.26	167	4.13	4.68	1.93	96
Jan 2011	4.29	4.84	2.37	85	3.23	3.65	2.11	41
Feb 2011	4.94	5.56	2.58	120	3.92	4.42	2.49	62
Mar 2011	4.96	5.59	2.65	119	4.01	4.53	2.35	69
Apr 2011	4.74	5.34	2.16	116	3.90	4.41	2.02	70
May 2011	4.55	5.12	2.62	88	3.83	4.32	2.46	55
Jun 2011	3.93	4.42	2.57	56	3.10	3.50	2.25	31
Jul 2011	3.80	4.26	2.76	47	2.93	3.32	2.27	26
Aug 2011	3.92	4.43	2.02	75	3.10	3.50	1.80	44
Sep 2011	3.64	4.09	2.76	42	2.92	3.29	2.45	24
Oct 2011	4.46	5.04	2.37	90	3.44	3.89	2.04	48
1 year	**4.43**	**5.00**	**2.32**	**92**	**3.52**	**3.98**	**2.08**	**52**

Table 1: Monthly measured wind statistics.

2.4 Wind Shear Estimation

Wind in the atmospheric boundary layer almost always increases with height (exceptions include nocturnal low level jets and complex topography induced circulations). A standard measure of the rate of wind speed increase with height is *wind shear exponent*, resulting from a power law fit to the vertical wind profile, given by

$$U(h) = U_0 \left(\frac{h}{h_0} \right)^{\alpha} \tag{2.2}$$

By trivial inversion of (2.2) the exponent α can be calculated directly for any two pairs of simultaneous speed and elevation records:

$$\alpha = \frac{\log(U / U_0)}{\log(h / h_0)} \tag{2.3}$$

The distribution of calculated instantaneous shear exponents from our filtered synchronized dataset (see Appendix 2) is shown in Figure 4a. Despite few anomalous high and low (negative!) shear values a clear peak of the distribution is observed. Figure 4b provides a zoomed in view and displays three possible single characteristic values. The mean shear is 0.48, the median is 0.41 and mode of the distribution is 0.34. Another single characteristic value of the shear exponent can be obtained by matching the directly measured mean WPD with the one calculated by extrapolation of wind speed data from another height. The value that allowed the best match is 0.36.

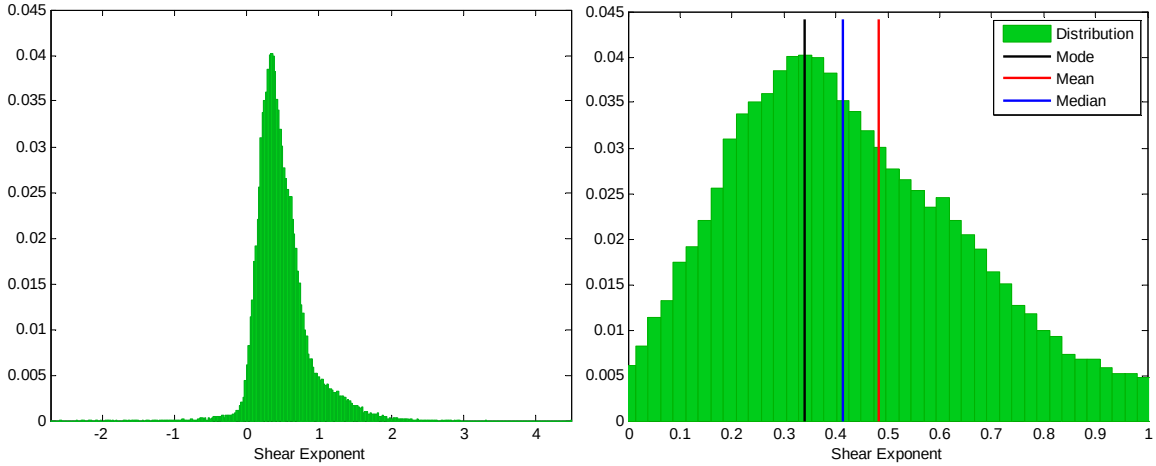

Figure 4: (a) Distribution of directly calculated instantaneous (10 minute averages) shear exponents.
(b) Enlarged view, mode, mean and median of the distribution.

2.5 Extrapolated Wind Power Density

A major source of uncertainty in wind resource assessment for wind power production is the vertical extrapolation to height at which direct measurements were not available. Due to the cubic nonlinearity of WPD dependence on wind speed, it is very sensitive to the uncertainty in extrapolation, as shown in the following table.

Elevation	20m	34m	50m	80m	100m
Shear=0.36	52.0	**92.0**	139	230	293
Shear=0.34	53.6	**92.0**	136	219	274
Shear=1/7	73.4	**92.0**	108	132	145
Upper bound	**51.7**	**92.0**	152	489	3647
Lower bound	92.15	**91.99**	91.81	91.48	91.26

Table 2: Mean WPD for one year extrapolated by various methods to different hub height. Numbers shown in bold are directly estimated mean WPD values without involving vertical extrapolation.

The first three rows are extrapolations with a single characteristic shear exponent. The value of 1/7 is a typical shear assumed in analyses when no better data is available. The upper bound is calculated with instantaneous (10 minutes averages) shear exponents, from Figure 4. The lower bound assumes there is no wind shear and the only variation is due to density decrease with height due to hydrostatic stratification of the atmosphere (calculated assuming isothermal exponential decay with height[1]).

The high uncertainty in the extrapolated WPD can be reduced by either direct measurements at higher elevations, remote sensing or numerical modeling.

[1] See the standard formula for air density calculation in *Wind Resource Assessment Handbook: Fundamentals for Conducting a Successful Wind Monitoring Program*, AWS Scientific, Inc., April 1997.

2.6 Directional Wind Distribution

An important aspect of understanding the nature wind resource at the site is the directional distribution of wind. The direction of wind is tied to the large scale meteorological phenomena producing the wind and is also affected by the local features of the site like topography, land roughness and tall obstacles. We present the directional distribution of wind by *wind rose* plots: the radial dimension represents the frequency of wind occurrence in each of the directional sectors. Each sector is divided to represent the absolute frequency of occurrence of wind speeds in this direction within speed intervals as represented by the color map.

The figures below show a clear dominance of northwesterly winds, blowing from Canada during winter season. Almost no wind is blowing from the east. The narrow band of frequent southeasterly winds, is probably associated with the sea breeze. The wide band of frequent southwesterly winds is associated with high pressure area in the mid-Atlantic states[1], which brings the fine weather to New England.

The slight gap due to reduction in speed and occurrence in the west-northwest direction at both heights may be associated with the local wake effect due to the water tower and the forest at the northwest of the meteorological tower. It may be also due to the obstruction to the larger scale flow by the elevated topographic shoulder and the higher hill 2000 feet to the west-northwest of the meteorological tower site.

Directional distribution of instantaneous (averaged over 10 minute periods) wind power densities (WPD) is shown in Figure 6. By and large the distribution corresponds closely to the wind speed distribution, while accounting for the nonlinear dependence of WPD on the wind speed. Wind power of more than 500 W/m^2 is common from all the directions, highlighting the need for an omni-directional wind harvesting device. What is not seen in the figure, due to limited resolution shown, is the low frequency occurrence of very high WPD events over 1000 W/m^2 and reaching over 2000 W/m^2 in only few instances. However, the contribution of these rare high wind events to overall wind energy potential and power production is small.

[1] *New England's Changing Climate, Weather, and Air Quality.* Climate Change Research Center, University of New Hampshire, 1998.

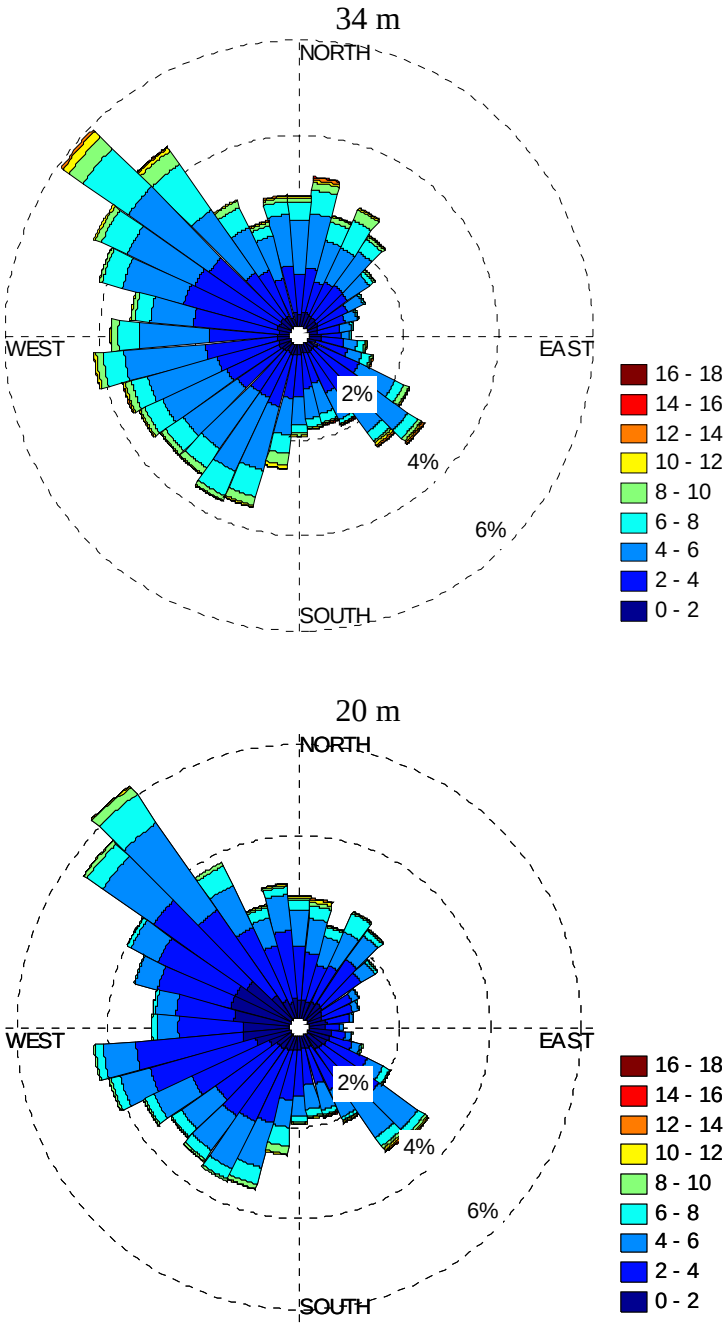

Figure 5: Wind rose of measured wind speed and direction, shown for two elevations 34 and 20 meters above ground. Wind direction by meteorological convention is the direction from which it is blowing.

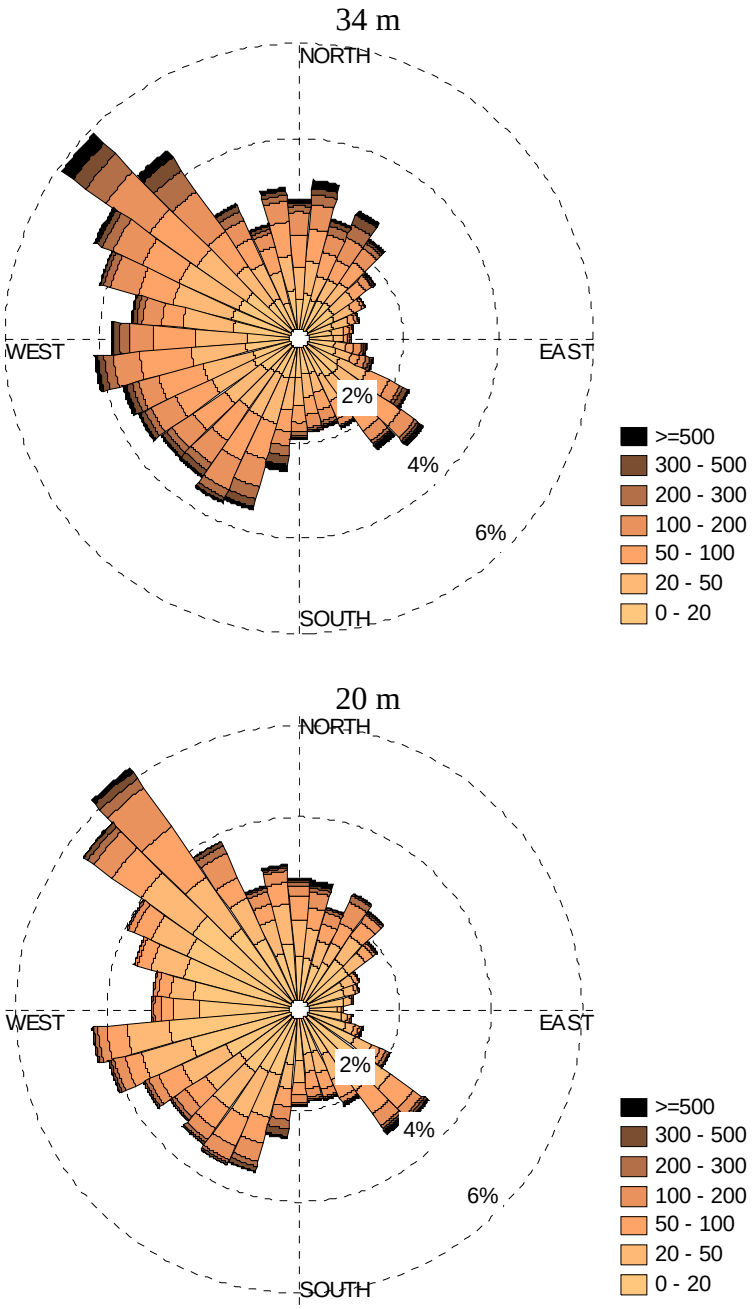

Figure 6: Wind rose of calculated wind power density (WPD) and direction, shown for two elevations 34 and 20 meters above ground.

3 Turbine Power Estimates

Selected small to medium size wind turbines were used for estimation of wind power production at the site. The specs of the turbines, taken from WEPA Danehy Park report[1], are listed in table 3.

	Skystream 3.7	Polaris 20	Northern Power 100	Aeronautica 29-225	Polaris 500
Manufacturer	Southwest Windpower	Polaris America	Northern Power Systems	Aeronautica Windpower	Polaris America
Rated Power [kW]	2.4	20	100	225	500
Hub Height [m]	20	36.6	37	50	50
Rotor Diameter [m]	3.7	10	21	29	50
Cutin / Cutout Speeds [m/s]	3.5 / 25	2.5 / 25	3.5 / 25	4 / 25	2.5 / 25
Rated Wind Speed [m/s]	13	10	14.5	15	12
Approximate Cost [$]	20,000	140,000	450,000	1,300,000	1,800,000

Table 3: Selected turbine specs.

Estimated annual power production (in kWh) and capacity factors (in %) for different turbines are shown in Table 4. Extrapolation to hub height of the turbines was done with two different shear estimates as listed in the table, the more conservative estimate is with the standard 1/7 shear exponent. In both cases the capacity factors increase significantly for the larger wind turbines.

Shear Estimate		Skystream 3.7	Polaris 20	Northern Power 100	Aeronautica 29-225	Polaris 500
Shear=0.36	Annual Energy Production [kWh]	**1,103**	17,980	102,700	243,200	786,750
	Annual Capacity Factor [%]	**5.24**	10.26	11.71	12.33	17.95
Shear=1/7	Annual Energy Production [kWh]	**1,103**	16,960	97,320	184,500	634,000
	Annual Capacity Factor [%]	**5.24**	9.67	11.10	9.36	14.46

Table 4: Selected turbines power production and capacity factors for different shear estimates. Numbers shown in bold are based on directly measured WPD values without involving vertical extrapolation.

[1] Chan C. et al., 2011. *Danehy Park wind turbine project preliminary assessment report*, WEPA, MIT.

Appendix 1: Met Tower configuration and calibration data

A. Anemometers

	Sensor 1	Sensor 2	Sensor 3	Sensor 4
• Serial Number	1021	1022	1016	1023
• Monitoring Height	34m	34.2m	20m	20.2m
• Primary / Redundant	20cm	20cm	20cm	20cm
• Mounting Orientation Degrees - Magnetic	268	124	268	124
• Boom Length	1.5m	1.5m	1.5m	1.5m
• Mount Above Boom				
• Calibrated by:	Otech	Otech	Otech	Otech
– Calibration Date	10/16/09	10/16/09	10/16/09	10/16/09
– Slope (mph/Hz)	0.759	0.758	0.757	0.759
– Offset (mph)	0.34	0.38	0.38	0.38
• Logger Terminal #	Ch 1	Ch 2	Ch 3	Ch 13
Comments:				

B. Wind Vanes

	Sensor 1	Sensor 2
• Monitoring Height	33m	19m
• Mounting Orientation Degrees - Magnetic	178	178
• Boom Length	1.5m	1.5m
• Mount Above Boom	20cm	20cm
• Deadband Orientation (º)	-2	-2
• Logger Terminal #	Ch 7	Ch 8
Comments:		

C. Temperature Sensor (NRG 110S)

• Monitoring Height	2m	• Slope / Offset (ºC)	default
• Mounting Orientation	300	• Logger Terminal #	Ch 9
Comments:			

D. NRG Data Logger

• Logger Type (√)	√ Symphonie Logger __ 9300 Cell Logger __ Wind Explorer		
• Logger Serial Number	428002590	• iPack Serial Number	n/a
• ESN Number	n/a	• Primary Internet Acct.	
• Phone Number		• Password of PIA	
• Phone Company		• Site Internet Acct.	
• SID Number		• Password	
• Home Type		• Average Interval	10 minutes
• Data Retrieval Method	Manual retrieval	• Retrieval Interval	
• Mounting Orientation		• Time Update ISP	
Comments:			

E. Tower Type

• Type	34m	• Height	34m
• Tower Diameter	6”	• Side Boom Diameter	0.5”
Comments:	8” x 7’ utility screw anchors. Top lays to 265 degrees. Gin pole and hardware left on site inside fenced area around watertower.		

Figure 7: Photograph of the installed meteorological tower.

Appendix 2: Data filtering and tower shadow effect

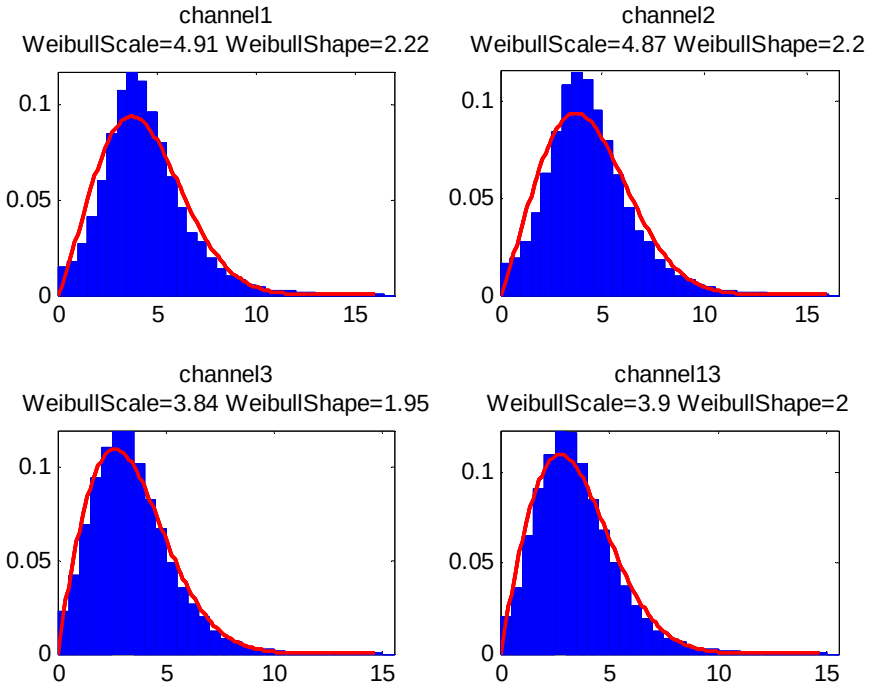

Figure 8: Unfiltered 10 minute average wind speed distribution and maximum likelihood Weibull fit for the 4 anemometer channels.

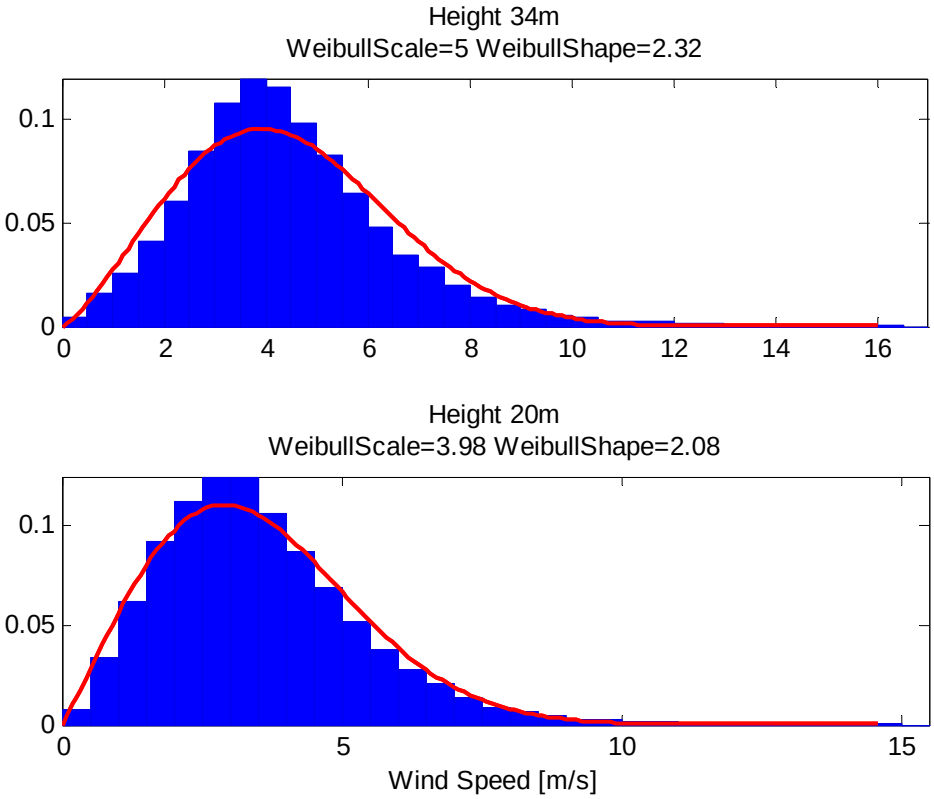

Figure 9: Filtered and synchronized wind speed data distribution and maximum likelihood Weibull fit at two heights.

Additional illustration of data analysis process is available in this appendix. The distribution of raw unfiltered 10 minute average wind speed data is shown in Figure 8 for the 4 anemometer channels. The maximum likelihood Weibull fit is overlaid on top, its parameters are given in the axes titles. The applied filters included icing conditions filtering based on zero standard deviations for 10 minute periods for all speed and direction channels. The effect of tower shadow is shown in Figure 10, which displays the difference between two channels at the same height as function of the direction measured by the vane at same height. At certain wind directions the difference between channels is higher than the typical random spread, meaning that one of anemometers must be in the wind shadow of the tower. These directions roughly correspond to the expected shadow angles based on the mounting orientation as listed in the tables in Appendix 1. The data resulting from icing filtering is also shown in Figure 10. The filtered data is shown by green symbols on top of the unfiltered raw data (blue symbols), showing that most of the anomalous points were eliminated. The shadow effect was filtered out by selecting the higher speed value recorded at the same height. The next filter applied selected only those time records when both upper and lower sensors had valid data. The resulting synchronized data set is necessary for shear calculation between the two heights. The histogram and Weibull fit of the final filtered synchronized data is shown in Figure 9. The expected reduction of low wind speed records is noticeable by the decrease in the height of the lowest wind speed bins at both heights.

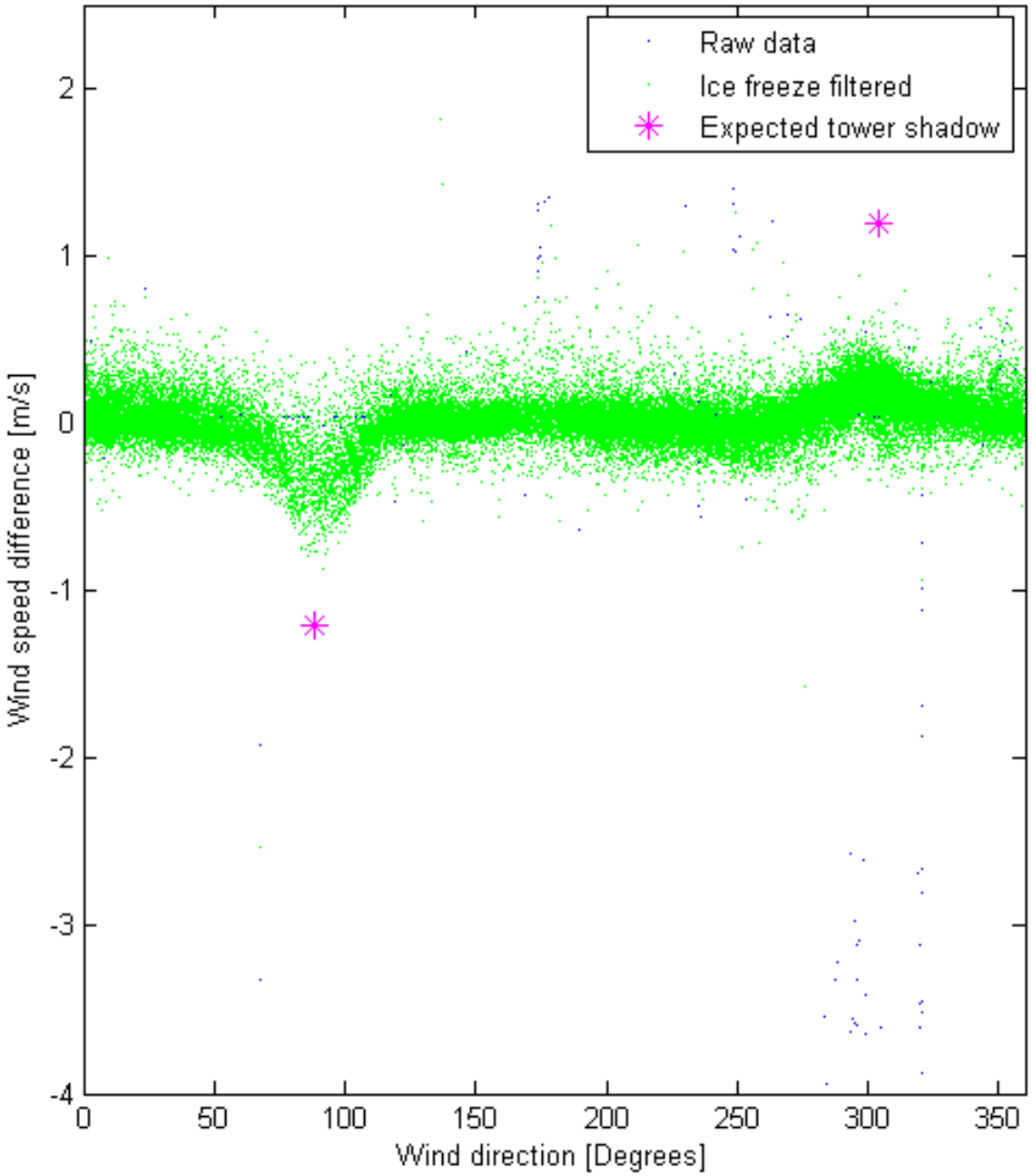

Figure 10: Tower shadow plot of raw unfiltered and filtered data for the upper sensors. Expected tower shadow directions are show by magenta symbols based on the sensors mounting orientation angles.

Appendix 3: NREL wind power classification and regional wind power map

Our estimate at 50m is: mean WPD 139 W/m^2 [±10%] which is well within "poor resource potential" wind power class 1.

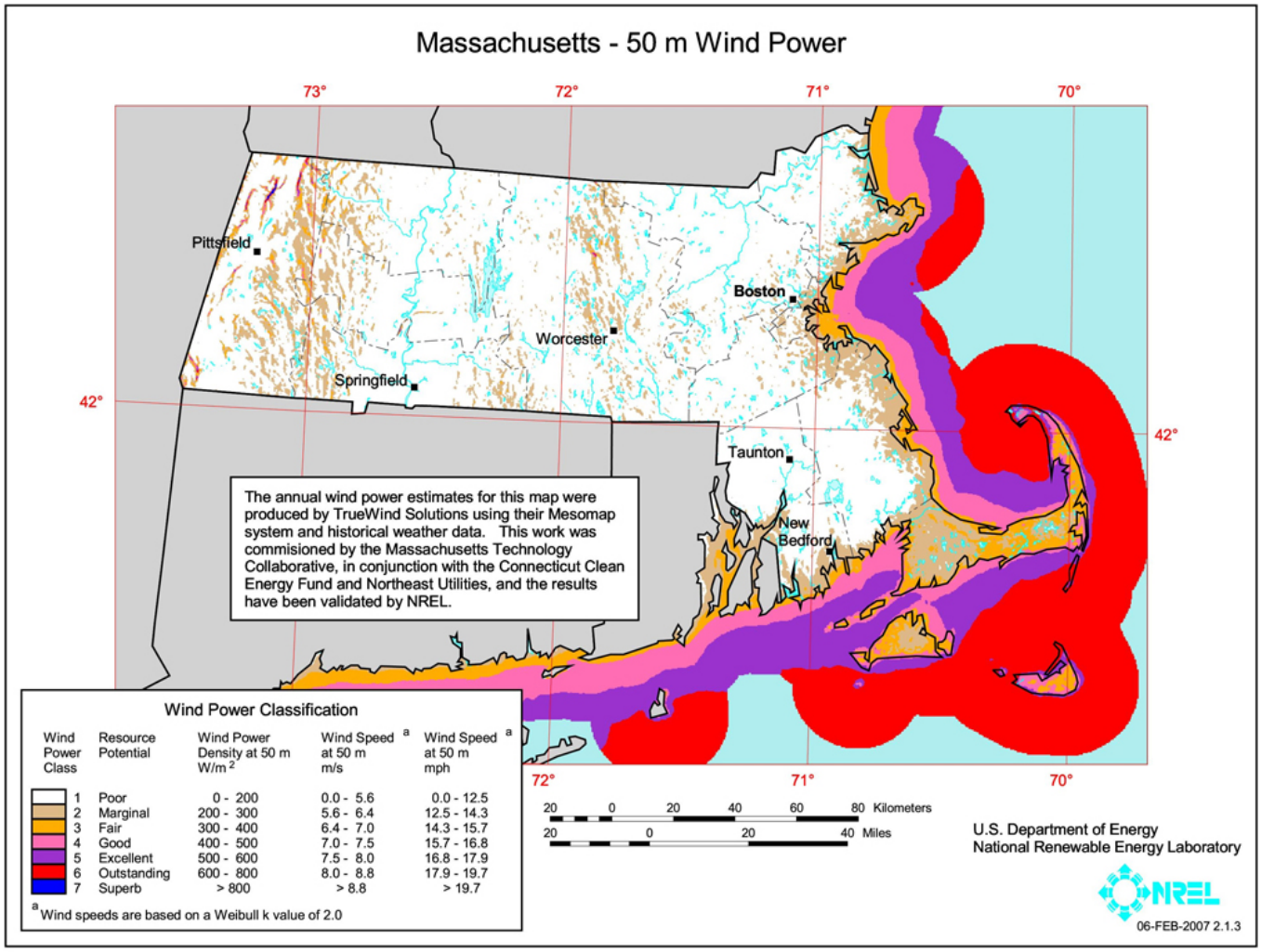

Figure 11: NREL Wind Power Class map of Massachusetts. Source: http://www.windpoweringamerica.gov/images/windmaps/ma_50m_800.jpg

Wind Power Class*	10 m (33 ft)		50 m (164 ft)	
	Wind Power Density (W/m^2)	Speed(b) m/s (mph)	Wind Power Density (W/m^2)	Speed(b) m/s (mph)
1	0	0	0	0
2	100	4.4 (9.8)	200	5.6 (12.5)
3	150	5.1 (11.5)	300	6.4 (14.3)
4	200	5.6 (12.5)	400	7.0 (15.7)
5	250	6.0 (13.4)	500	7.5 (16.8)
6	300	6.4 (14.3)	600	8.0 (17.9)
7	400	7.0 (15.7)	800	8.8 (19.7)
	1000	9.4 (21.1)	2000	11.9 (26.6)

Table 5: Standard NREL Wind Power Classification table for 10 and 50 meter heights.

4 Shadow Flicker

4.1 Introduction

In terms of environmental and community impact, shadow flicker generated by wind turbines on the nearby residential community can be a potentially serious problem. Specifically, shadow flicker results when sunlight passes behind rotating turbine blades, resulting in alternating light intensities cast on stationary objects (*1*). Residential buildings within the shadow flicker zone will experience alternating changes in light reception in rooms facing the wind turbine (*2*), and the intensity of the shadow flicker will be determined by various factors including the angle and intensity of the sunlight, distance from the turbine, and the blade rotation frequency. An illustration of the shadow flicker effect is shown in Figure 1. According to the United Kingdom *Planning for Renewable Energy Guide*, shadow flicker effects have only been reported to occur within 10 rotor diameters of the turbine (*1*). Thus, to avoid residential impact, a typical conservative recommendation is to site turbines at least 10 rotor diameters away from the nearest occupied dwelling.

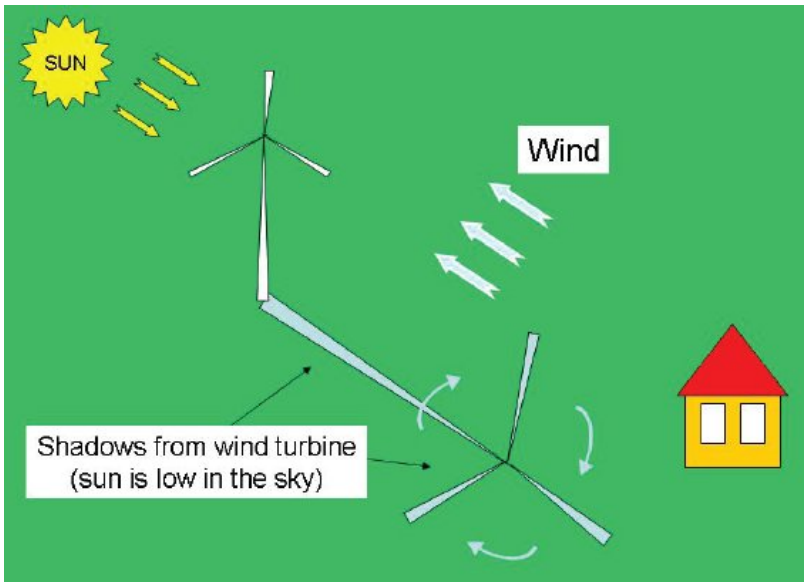

Figure 1. Illustration of shadow flicker caused by rotating turbine blades (not to scale) (*3*)

4.2 Computational Model

As the sun moves across the horizon each day, the shadow flicker will shift with the changing angle of the sunlight. Furthermore, changing sun paths with the seasons will affect the angle at which sunlight hits the turbine blades. Sun paths at the tower site for January through June and July through December are shown in Figures 2 and 3, respectively. As indicated by the figures, elevation of the sun above the horizon shifts seasonally. The changing sun trajectories entail that a shadow flicker zone exists in which dwellings within the zone may be affected at specific times of the year. The flicker zone was modeled for a turbine height of 34 meters using the following assumptions (*4*):

1. The wind speed is assumed constant as a mean speed (i.e. no seasonal variation of wind speed)
2. The wind blades are rotating in a constant rotational speed that is corresponding speed to the mean wind speed
3. The wind turbine blade is considered to be a 2-dimensional circular disk element by its swept area.
4. The disk element is always normal to the sun light direction
5. The weather is in a perfect condition with a sufficient sun light all time during the day, and the sky is 100% clear with no allowance for mist, fog, cloud etc.
6. There are no obstacles along the line of sight between the receiver and turbine blade
7. The Sun can be considered as a point light source
8. The sun has to be 5 degrees above the horizon in order to be seen and creates shadow

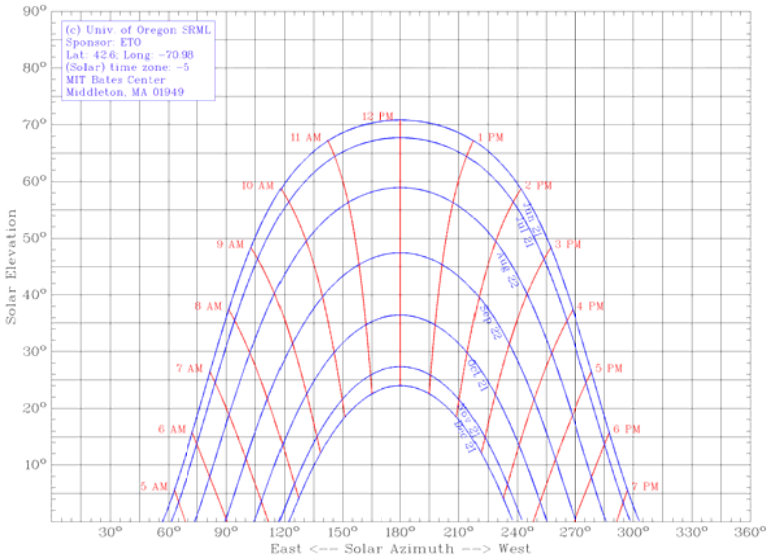

Figure 2. Sun trajectories at MIT Bates for January through June (*5*)

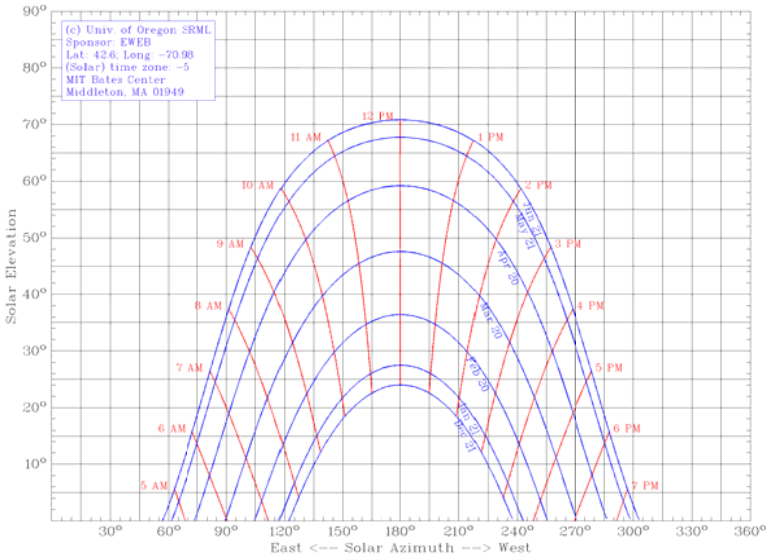

Figure 3. Sun trajectories at MIT Bates for July through December (*5*)

Using data from the sun paths, a 3D plot of the sun trajectory and the corresponding shadow flicker zone on the ground can be generated (figure 4). Figure 5 shows the shadow flicker zone from above, which is projected to have a butterfly shape.

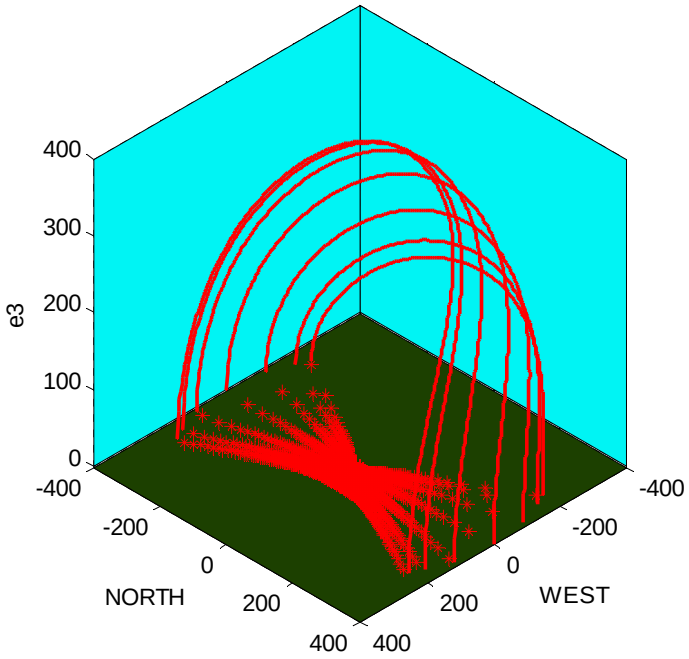

Figure 4. 3D view of sun trajectory paths and projected shadow flicker zone on ground (units shown on axes are in meters)

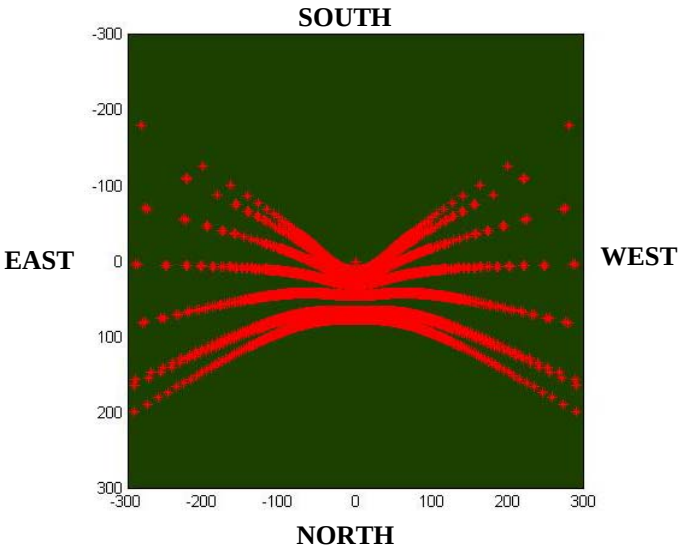

Figure 5. Projected shadow flicker zone (units shown on axes are in meters)

4.3 Analysis of Community Impact

Figure 6 displays the potential zone affected by the shadow flicker at the turbine site for a turbine height of 34 meters. It should be noted, however, that the shadow flicker zone is an over-estimated area due to the computational assumptions of 100% clear skies and a blade-swept area normal to the sun (*4*).

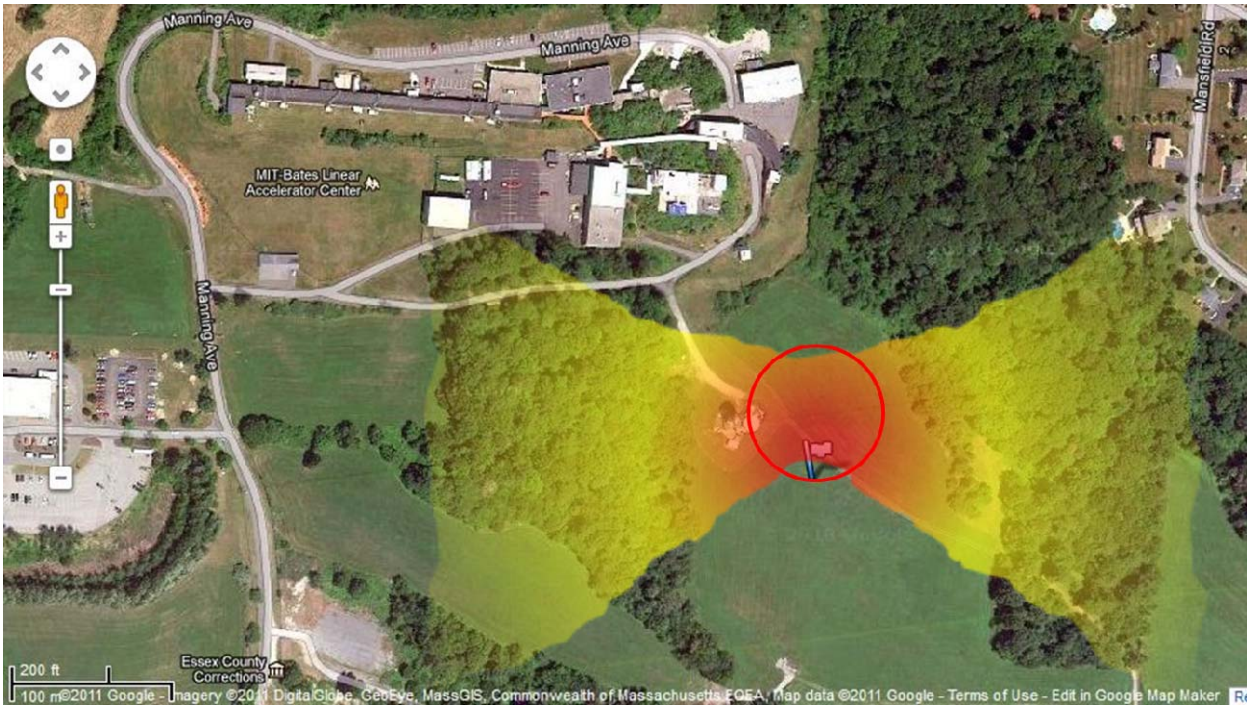

Figure 6. Projected area affected by shadow flicker for turbine at +42° 35' 47.73", -70° 58' 42.40 (6)

It is known that flickering becomes less distinct with increasing distance away from the turbine (*1*), and that beyond a distance of 10 rotor diameters from the turbine, blade rotation is simply perceived as an object in front of the sun (*4*). The further away from the turbine, the more diffuse the shadow becomes. Consequently, the actual zone of perceivable flicker will be concentrated to the circle drawn in Figure 6. The shadow flicker generated by the turbine will most likely not have a significant impact on the community as no receptors are within the zone of perceivable flicker.

In terms of health and safety, the impact of the shadow flicker will be negligible. One potential concern is the shadow flicker effect on those with photosensitive epilepsy. However, the frequency at which turbine blades rotate (0.5-1.25 Hz (*3*)) is below the range that triggers seizures (generally 5-30 Hz) and therefore does not represent a threat to epileptics and other photosensitive persons (*7, 8*). In the event that shadow flicker is determined to be a nuisance, the effects may be mitigated by planting vegetation such as trees to provide an obstruction between the flicker and impacted dwelling, covering windows and/or switching lights on indoors during periods when shadow flicker occurs.

References

1. Nielsen, Arne. Wind Engineers Inc. “Initial Shadow Flicker Modeling Results, Kittia Valley Wind Power Project, WA.” April 20, 2003.

2. Wehler, Bryan M. ARM Inc. “Frey Farm Landfill (FFLF) Wind Energy Project – Shadow Flicker Analysis.” December 9, 2009.

3. Noble Environmental Power, LLC. “Wind Fact Sheet #4: Shadow Flicker.” Web. http://www.noblepower.com/faqs/documents/06-08-23NEP-ShadowFlicker-FS4-G.pdf

4. Lee, Sungho. “Preliminary Results of Shadow Flicker and Sound Analysis.” March 1, 2010.

5. Sun Path Chart Program. University of Oregon Solar Radiation Monitoring Laboratory. Web. http://solardat.uoregon.edu/SunChartProgram.php

6. Google Maps. Web. http://maps.google.com

7. American Wind Energy Association. “Wind Turbines and Health.” Web. http://www.awea.org/documents/factsheets/Wind_Turbines_and_Health.pdf 28 Feb. 2011

8. “Photosensitivity and Epilepsy.” Epilepsy Foundation. Web. http://www.epilepsyfoundation.org/about/photosensitivity/ 28 Feb. 2011